

## Research Paper

# Analysis and Optimization of Radiant Cooling Panel with Wave-Type Embedded Pipes

Ramprasad PRASANNA<sup>1</sup>, Prakash MOORTHY<sup>1,2\*</sup>, Aravind KRISHNAN<sup>1</sup>  
Venkatesh BALAKRISHNAN<sup>1</sup>

<sup>1)</sup> *School of Mechanical Engineering  
SASTRA Deemed University, Thanjavur  
Tamil Nadu, India, 613 401*

<sup>2)</sup> *Centre for Energy Storage & Conversion  
SASTRA Deemed University, Thanjavur  
Tamil Nadu, India, 613 401*

\*Corresponding Author e-mail: prakash@mech.sastra.edu

In this study, the radiant cooling panel with wave-type pattern pipes is analyzed and optimized through Taguchi's design of experiments methods and grey relation method for better performance. Radiant cooling panel's bottom surface temperature and temperature non-uniformity index are considered as the quality objective functions. Control parameters such as pipe length, the spacing between the pipes, radiant panel thickness, pipe bent radius, pipe diameter, insulation layer thickness, pipe material, panel material, insulation material, and mass flow rate of water entering the pipe are included as the control parameters of the optimization study. The performance of radiant cooling panels is analyzed through numerical simulation technique- computation fluid dynamic (CFD) method. The numerical simulation is carried out in the Fluent software, and the CFD code is checked for grid independence and validation. Through single and multi-objective optimization, the best design of the radiant cooling panel is identified, and a confirmation test is also conducted. Finally, an analysis of variance (ANOVA) calculation is made and it is found that the mass flow rate of water entering the pipe is the most influencing parameter on the performance of the radiant cooling panel.

**Key words:** radiant cooling panel; optimization; computational fluid dynamics; ANOVA.

## 1. INTRODUCTION

In the last two decades, energy and environmental-related problems along with global warming have increased the attention on the development of passive cooling techniques in the buildings. Especially, cooling appliances in buildings in the hot climate regions consume high energy through air coolers and air conditioners to maintain the indoor thermal comfort of occupants. Many countries are making an effort in the development of the passive integral conditioning system

to balance the energy demand. In this context, a radiant cooling system has become popular since it offers good indoor comfort with zero energy consumption. Some Japanese hospitals adopted a ceiling cooling system and also observed that 30% of energy consumption could be saved by using a radiant cooling system in comparison with a conventional HVAC system [1]. Radiant cooling panel system exchanges heat by radiation and convective mode of transfer by utilizing the surrounding surfaces as cooling surfaces. Commonly used radiant cooling systems include radiant ceiling cooling [2], cooling ceiling [3], radiant cooling ceiling system [4], ceiling radiant cooling panel [5], radiant chilled panel system [6], and suspended metal ceiling radiant system [7]. In most of the radiant cooling panel system, the tubes are embedded in the screed [8], urethane foam material [2], concrete slab [9–11], gypsum [12, 13], and gramolyth [13]. The arrangement of embedded pipes in the cooling panel influences the panel's cooling capacity and the uniformity in temperature distribution over the panel surface. ARCURI *et al.* [35] used a set of parallel pipes, ZHANG *et al.* [11] used two circuits of S-shaped pipes being offset for a certain distance, and XIE *et al.* [14] used U-shaped capillary pipes, CHOLEWA *et al.* [13] employed spiral type of pipes in their study on radiant cooling panel. XIE *et al.* [14] analyzed the temperature non-uniformity by varying the parameters such as inlet water temperature, tube spacing, plaster thickness, thermal conductivity, and observed that it directly depends on tube spacing. Also, most of the studies on the radiant cooling panel were conducted for the residential buildings [15–18], office buildings [4, 19], and educational buildings [20, 21]. The performance of the radiant cooling system was estimated through cooling capacity [5, 6], indoor thermal comfort index [15, 22], average temperature [9, 23], heat transfer coefficient [13, 24] and temperature non-uniformity index [14]. Also, the performance of the radiant cooling system was analyzed through field study [19, 20], CFD method [4, 25, 26], lab test [22, 26], simulation [15, 27], CFD with field study [28], CFD with lab test [29], and simulation with lab test [17]. SHEN *et al.* [37] conducted an optimization and parametric study on thermoelectric radiant cooling and heating panel and included a number of thermoelectric modules and the thickness of the radiant panel as design variables. Since the latter study considered only two design factors, the authors employed a full factorial approach for optimization and found the optimum value for panel thickness as 4 mm and a number of thermoelectric modules as 16 per square meter. ROMANI *et al.* [38] optimized the deterministic controls for a cooling radiant wall through a generalized pattern search (GPS) Hooke-Jeeves with the single seed optimization algorithm. In this study, the author reported that solar control concepts maximized the self-consumption of renewable energies in the building, and thereby the goals of net-zero energy buildings were achieved. JOE and KARAVA [39] introduced a smart operation strategy based on model predictive control (MPC) to optimize the performance of hydronic radiant floor systems

in office buildings. The MPC approach uses dynamic estimates and predictions of zone loads and temperatures, outdoor weather conditions, and HVAC system models to minimize energy consumption and cost, while meeting equipment and thermal comfort constraints and producing an energy saving of 29–50%.

In the above review, we learned about the influence of various geometrical parameters and pipe patterns on the performance of the radiant cooling panel and the methods employed to analyze its performance. Also, the implementation of an optimization technique in the radiant cooling panel was identified as very limited.

With this information, the present work aims to analyze and optimize a radiant cooling panel with wave-type pipe pattern through computational fluid dynamics technique. In the optimization of the cooling panel, parameters that influence the performance of the cooling panel should be identified and a full factorial test is required to identify the best values for the influencing parameter. However, the full factorial test takes high number of experimental runs. In this context, optimization techniques such as the design of experiments (DOE) and the grey relational method greatly reduce the number of experimental runs, and hence, in this work, the above methods are employed.

## 2. RADIANT COOLING PANEL

In the radiant cooling panel, pipes with wave shape are embedded in the gypsum layer of 0.05 m thickness. The gypsum layer is insulated with the cellulose of 0.01 m thickness, laid above the gypsum layer to restrict the heat transfer via outdoor and concrete. This panel is attached underside of the concrete of 0.15 m thickness. The wave-shape tubes are made of copper with a diameter of 0.02 m, the thickness of 0.00075 m, and the bend radius of 0.03 m. In one panel, five tubes are placed in a parallel way with a spacing of 0.06 m. The length of each pipe is 1.2 m, the total length of the pipe is about 6 m, and each pipe is made with twelve bends. Each bend has an angle of  $180^\circ$  and its length measures about 0.09425 m. The panel size measures about  $0.33 \times 0.772 \times 0.06$  m (width  $\times$  length  $\times$  height) excluding top concrete layer. The performance of the radiant cooling system is analyzed by numerical simulation technique- computation fluid dynamics since the CFD technique is widely used in the prediction of indoor heat transfer and thermal comfort of buildings.

## 3. NUMERICAL SIMULATION METHODOLOGY

The radiant cooling panel attached to the roof is shown in Fig. 1, and is modeled in a three-dimensional approach. Though the performance of the cooling panel largely depends on the outdoor and indoor conditions, the air surrounding

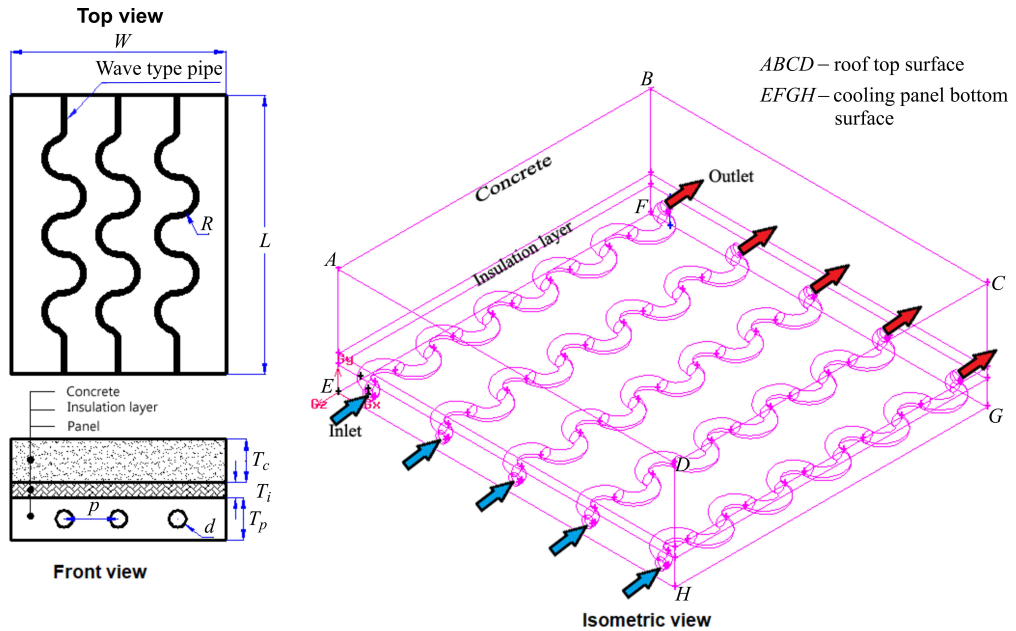


FIG. 1. The geometry of the radiant cooling panel with wave-type pipes.

the panel is not modeled for the sake of simplicity. This kind of simplification consumes less number of mesh cells and time for solving, without sacrificing the accuracy of the simulation. However, the conditions of the outdoor and indoor air are defined as the boundary conditions over the model.

### 3.1. The physical and mathematical model

The physical model of the radiant cooling panel contains the concrete layer, insulation layer, and panel with embedded pipes. Both fluid flow and associated heat transfer phenomenon are considered in this model. The physical model is created in the Design Modeler software ANSYS. First, the convective heat transfer occurs between water and the pipe internal surface, and conduction of heat takes place across the pipe and panel. Finally, the combined heat transfer of convection and radiation occurs on the panel surface with the room indoor. The assumptions involved in this analysis are given below:

- (i) Thermophysical properties of water and other panel materials are constant.
- (ii) Flow is incompressible.
- (iii) Sidewalls of the panel are adiabatic.
- (iv) Thermal contact resistance is negligible.
- (v) Heat transfer is steady-state and the accumulation of heat is negligible.

The governing equations associated with this study are continuity, momentum, and energy conservation, and these equations are solved by Fluent – ANSYS. Equations (3.1)–(3.3) govern the flow of fluid in the embedded pipe, and Eq. (3.4) corresponds to the heat transfer in the radiant cooling panel:

$$(3.1) \quad \frac{\partial}{\partial X_i} (\rho_w U_i) = 0,$$

where  $\rho_w$  is the water density,  $X$  is the coordinate axis in the direction  $i$  ( $i = 0, 1, 2$ ).  $U_i$  refers to the mean velocity in the  $i$ -th direction:

$$(3.2) \quad \frac{\partial (\rho_w U_i U_j)}{\partial X_i} = \frac{\partial P}{\partial X_j} + \mu \frac{\partial}{\partial X_i} \left( \frac{\partial U_i}{\partial X_j} + \frac{\partial U_j}{\partial X_i} \right),$$

where  $P$  is the pressure, and  $\mu$  is the kinematic viscosity of water

$$(3.3) \quad \frac{\partial (\rho_w U_i T)}{\partial X_i} = \frac{\gamma}{C_p} \frac{\partial}{\partial X_i} \left( \frac{\partial T}{\partial X_i} \right),$$

where  $T$  is the temperature,  $\gamma$  is thermal conductivity, and  $C_p$  is the specific heat.

The equation that governs the heat transfer across the concrete, insulation wall and cooling panel is given in Eq. (3.4):

$$(3.4) \quad \frac{\partial}{\partial X_i} \left[ K_i \frac{\partial T}{\partial X_i} \right] = 0,$$

where  $K_i$  is the thermal conductivity,  $\frac{\partial T}{\partial X_i}$  is the temperature gradient in the direction  $i$  ( $i = 0, 1, 2$ ).

The boundary conditions defined over the geometric model are as follows:

- (i) Pipe inlet: The mass flow rate of water entering the pipe is specified as 0.001 kg/s, and the temperature is equivalent to 300 K.
- (ii) Rooftop surface (ABCD): Rooftop surface is exposed to both solar radiation and convection by surrounding air. The combined effect of radiation and convection over the rooftop surface is defined by an equivalent temperature  $T_{\text{sol-air}}$  [36].  $T_{\text{sol-air}}$  is calculated at 12 PM for the month of May in the city Chennai, India from Eq. (3.10) and specified as a Neumann boundary condition (Eq. (3.5)) on the rooftop surface

$$(3.5) \quad q_{co} = h_o (T_{\text{sol-air}} - T_r),$$

where  $h_o$  is the outdoor heat transfer coefficient, and  $T_r$  is the mean temperature of the rooftop surface:

$$(3.6) \quad T_{\text{sol-air}} = T_a + \frac{\alpha q}{h_{co}},$$

where  $T_a$  is the outdoor temperature, the  $\alpha$  absorptivity of the roof surface,  $q_{is}$  is the solar radiation, and  $h_{co}$  is the outdoor convective heat transfer coefficient.

- (iii) Panel bottom surface (EFGH): Cooling panel bottom surface is exposed to room indoor, and hence the surface is subjected to convective heat transfer only. Convective heat transfer coefficient of  $4.27 \text{ W}/(\text{m}^2 \cdot \text{K})$  and an assumed indoor temperature of  $300 \text{ K}$  are specified as a Neumann boundary condition:

$$(3.7) \quad q_{ci} = h_i (T_i - T_{pm}),$$

where  $h_i$  is the convective heat transfer coefficient of indoor space,  $T_i$  is the indoor room temperature, and  $T_{pm}$  is the mean cooling panel bottom surface temperature.

- (iv) All lateral surfaces of the model are defined as adiabatic with free slip condition.
- (v) At the interface between the fluid and the internal wall of the pipe, the heat transfer in the fluid is coupled with conductive heat transfer throughout the pipe.

### 3.2. Material properties

The thermophysical properties of various elements in the radiant cooling panel are given in Table 1.

**Table 1.** Material properties of various elements in the radiant cooling panel.

Materials	Density [ $\text{kg}/\text{m}^3$ ]	Specific heat [ $\text{J}/(\text{kg} \cdot \text{K})$ ]	Thermal conductivity [ $\text{W}/(\text{m} \cdot \text{K})$ ]
Water	998.2	4182	0.6
Gypsum	2320	1138	0.5
Concrete	2300	880	1.4
Polystyrene	55	1210	0.027
Screed/cement Mortar	1860	780	0.72
Cork	160	1900	0.0525
Cellulose	45	1400	0.039
Steel	8030	502.48	16.27
Copper	8978	381	387.6
Aluminum	2719	871	202.4

### 3.3. Meshing and solution methodology

The model is meshed with the tetrahedral T-grid type of element since tetrahedral elements fit better for complex geometry than hexahedral elements. The grid spacing of 0.01 is employed for meshing the model, it consumes about 400 000 cells, and the mesh size is also checked for grid independence. The flow domain is solved under the  $k$ - $\varepsilon$  turbulence model with a second-order upwind scheme for discretization. The semi-implicit pressure linkage method is employed to couple the flow velocity and pressure. All the simulation cases are iterated up to the convergence level of  $10^{-6}$ .

### 3.4. Validation of CFD simulation

This numerical simulation is validated with the temperature non-uniformity coefficient predicted for the capillary ceiling radiant cooling panel system. The temperature non-uniformity index  $C_t$  is the ratio of root mean square deviation of temperature to the mean surface temperature, which is calculated through Eqs (3.8)–(3.10). This nonuniformity index should be minimum, to provide a uniform temperature at the panel surface, and thereby reducing condensation risk

$$(3.8) \quad C_t = \frac{\sigma_T}{T_m},$$

$$(3.9) \quad \sigma_T = \sqrt{\frac{\sum_{i=1}^N (T_i - T_m)^2}{N}},$$

$$(3.10) \quad T_m = \frac{\sum_{i=1}^N T_i}{N}$$

where  $T_i$  is the temperature recorded at  $N$  number of discrete locations on the radiant cooling panel surface.

The capillary ceiling radiant cooling panel includes a capillary tube of U-type embedded in the gypsum layer with an insulation layer at the top. This model is simulated for the boundary conditions of chilled inlet water temperature of 16–20°C, for a water velocity = 0.05 m/s and 0.3 m/s, the pipe diameter of 4 mm, tube spacing of 20 mm and gypsum layer thickness of 10 mm (see XIE *et al.* [14]). The temperature non-uniformity index is calculated through Eq. (3.9) and compared with the results predicted by XIE *et al.* [14]. It is found out that this numerically simulated temperature non-uniformity index is in a good agreement with XIE *et al.* [14] result as shown in Fig. 2. By validating the CFD simulation, the same methodology is applied to the radiant cooling panel with wave-type pipe

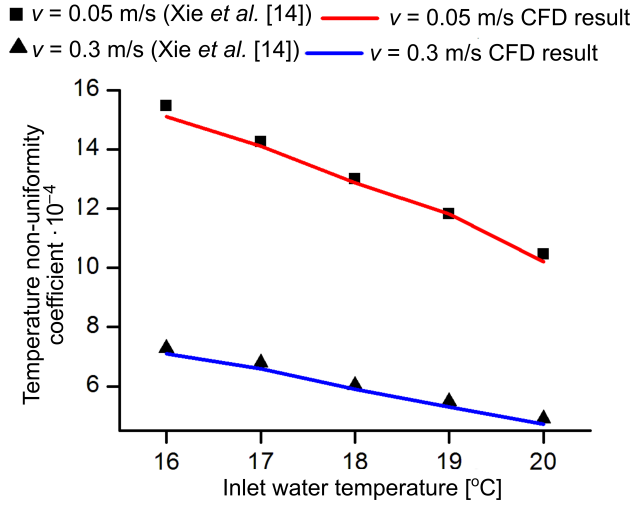
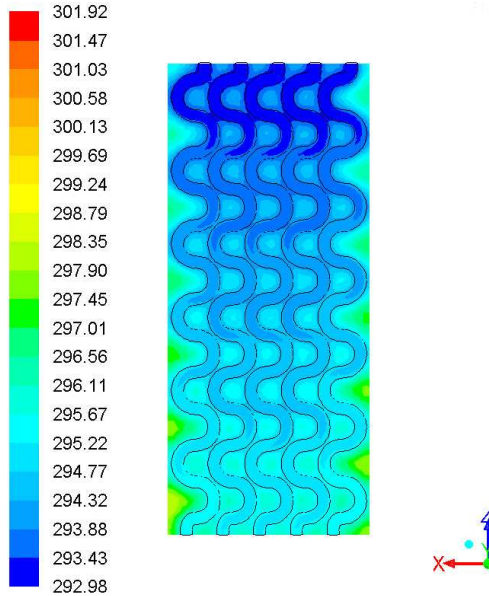


FIG. 2. Validation of CFD simulation.

pattern, and as an outcome of CFD simulation, the temperature distribution on the  $XZ$  plane at  $Y$  of 0.025 m is shown in Fig. 3 as a sample result.

FIG. 3. Temperature distribution at  $Y$  of 0.025 m.

The above radiant cooling panel is optimized under single and multi-objective functions for better performance through Taguchi's technique.

## 4. OPTIMIZATION BY TAGUCHI'S DESIGN OF EXPERIMENT TECHNIQUE

In earlier days, to optimize any function a full factorial test has been conducted. This full factorial test required a greater number of experimental tests to arrive at the optimum solution. Say, if four parameters are influencing the system, and these four factors are varied to three different values, then the full factorial test requires 81 possible combinations to test. In this context, Dr. Genichi Taguchi, a Japanese quality management consultant, proposed a specially designed orthogonal array (OA) to study the entire parameter space with a small number of experiments only [31]. Hence, this technique became one of the most powerful methods used in both engineering and non-engineering applications to achieve the desired quality at the earliest time. The success of the Taguchi's technique is behind the orthogonal array and the loss function. The orthogonal array generates a series of well-planned experiments with simultaneous variation in parametric values, and hence, a smaller number of experiments are required in comparison with the full factorial test. Also, the Taguchi method calculates the loss function as the difference between the experimental and desired values. This loss function is considered as signal-noise (S/N) ratio [32], where signal and noise represent controllable and uncontrollable factors. Here, the controllable and uncontrollable factors refer to the factors that influence and do not influence the objective function, respectively. The methodology of Taguchi's optimization technique is shown in Fig. 4.

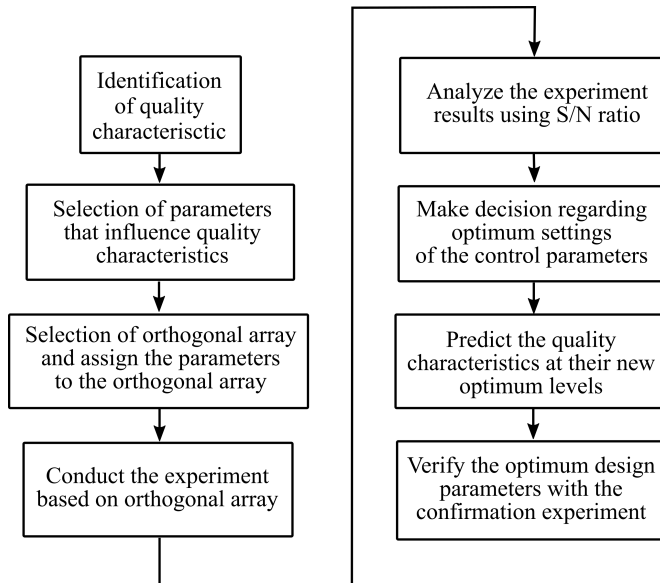


FIG. 4. Flow chart for Taguchi's optimization method.

In this study, the radiant cooling panel discussed in Sec. 2 is optimized for better performance. The average temperature at the bottom of the radiant cooling panel and the temperature non-uniformity index is the two-quality characteristic factor that determines its performance. The average temperature at the radiant cooling panel bottom is generalized with the indoor temperature as  $T^*$ , which is determined from Eq. (4.1) and temperature non-uniformity index coefficient  $C_t$  from Eq. (3.5).

$$(4.1) \quad T^* = \frac{T_i}{T_p}.$$

#### 4.1. Identification of quality characteristics and control parameters

The quality objective function for  $T^*$  should be maximum so that the average temperature of the panel bottom should be minimum and makes the indoor thermally comfortable. Temperature non-uniformity index coefficient,  $C_t$  should be minimum so that the risk due to condensation should be avoided. Based on the quality objective, the equation to determine the S/N ratio selected as the larger is best and as the smaller is best for the maximization and minimization of the quality objective function, respectively. The parameters that affect the above quality functions are identified as pipe length, the spacing between the pipes, radiant panel thickness, pipe bent radius, pipe diameter, insulation layer thickness, pipe material, panel material, insulation material, and mass flow rate of water entering the pipe. These ten parameters are varied through three levels of values and are given in Table 2.

**Table 2.** Parameters and three levels of value.

Parameter	Level 1	Level 2	Level 3
Pipe length ( $L$ )	5 m	10 m	15 m
Pipe spacing ( $P$ )	0.15	0.2	0.25
Panel thickness ( $T_{pa}$ )	0.05	0.075	0.1
Pipe bend radius ( $R$ )	0.03	0.05	0.07
Pipe diameter ( $d$ )	0.02	0.0225	0.025
Insulation layer thickness ( $T_i$ )	0.02	0.035	0.05
Pipe material ( $M_p$ )	copper	aluminum	steel
Panel material ( $M_{pa}$ )	concrete	gypsum	screed
Insulation material ( $M_i$ )	cellulose	polystyrene	cork
Mass flow rate of water ( $m$ )	0.001	0.003	0.005

#### 4.2. Selection of orthogonal array and analysis of results

The orthogonal array is a special design made by Taguchi to study the entire parameter space with only a small number of experiments. While selecting the suitable orthogonal array, the number of degree of freedom of orthogonal array (OA) should be greater than or at least equal to those for the process parameter [29]. In this study, the number of degrees of freedom for the process parameter is equal to 20, and hence the OA should be selected in such a way that the degree of freedom of OA must be greater than 20. From the available standard orthogonal arrays, the L27 orthogonal array is selected since it has 26 degrees of freedom and can handle up to thirteen parameters with three levels of variation. The identified control parameters are assigned in the L27 array and analyzed through a numerical simulation method for the boundary conditions stated in Sec. 2. From the numerical analysis, the average temperature at the radiant cooling panel bottom surface and the temperature at twelve discrete points of ceiling surface are recorded. The twelve locations are at equal distance in both directions. The two output responses  $T^*$  and  $C_t$  are predicted from the numerical simulation results and shown in Table 3. The corresponding  $S/N$  ratio is calculated based on the larger is the best and the smaller is the best Eqs (4.2) and (4.3), and it is given in Table 3:

- larger is the best equation:

$$(4.2) \quad S/N = -10 \log \left( \frac{1}{n} \sum_{i=1}^n \frac{1}{y^2} \right),$$

- smaller is the best equation:

$$(4.3) \quad S/N = -10 \log \left( \frac{1}{n} \sum_{i=1}^n y^2 \right),$$

where  $n$  is the number of trial cases and  $y$  is the output responses.

The mean effects plots for the  $S/N$  ratio of  $T^*$  and  $C_t$  are shown in Figs 5 and 6, respectively.

From the mean of the  $S/N$  ratio plot for  $T^*$  and  $C_t$ , the best value of the respective parameter is identified as the peak value of the mean of the  $S/N$  ratio from the three levels of variations. The best level value and influence rank of the parameters for the output response  $T^*$  and  $C_t$  are given in Table 4. In Table 4, the rank represents the parameter that has more influence on the objective function.

**Table 3.** The L27 orthogonal array with output responses  $T^*$  and  $C_t$  values and  $S/N$  ratio values.

Ex. No	$L$	$P$	$T_{pa}$	$R$	$d$	$T_i$	$M_p$	$M_{pa}$	$M_i$	$m$	$T^*$	$C_t \cdot 10^{-4}$	$S/N$ ratio $T^*$	$S/N$ ratio $C_t$
1	1	1	1	1	1	1	1	1	1	1	1.090	5.11	0.747	45.83
2	1	1	1	1	2	2	2	2	2	2	1.202	1.46	1.598	56.69
3	1	1	1	1	3	3	3	3	3	3	1.237	1.08	1.848	59.32
4	1	2	2	2	1	1	1	2	2	2	1.117	2.03	0.960	53.85
5	1	2	2	2	2	2	2	3	3	3	1.167	1.61	1.339	55.88
6	1	2	2	2	3	3	3	1	1	1	1.122	3.84	0.997	48.30
7	1	3	3	3	1	1	1	3	3	3	1.078	2.47	0.655	52.15
8	1	3	3	3	2	2	2	1	1	1	1.050	4.46	0.428	47.01
9	1	3	3	3	3	3	3	2	2	2	1.117	2.00	0.957	53.96
10	2	1	2	3	1	2	3	1	2	3	1.219	1.74	1.720	55.21
11	2	1	2	3	2	3	1	2	3	1	1.028	5.33	0.237	45.46
12	2	1	2	3	3	1	2	3	1	2	1.108	3.54	0.891	49.03
13	2	2	3	1	1	2	3	2	3	1	0.983	5.26	-0.152	45.58
14	2	2	3	1	2	3	1	3	1	2	1.134	2.47	1.090	52.14
15	2	2	3	1	3	1	2	1	2	3	1.148	2.84	1.202	50.95
16	2	3	1	2	1	2	3	3	1	2	1.069	3.87	0.577	48.25
17	2	3	1	2	2	3	1	1	2	3	1.190	2.40	1.508	52.40
18	2	3	1	2	3	1	2	2	3	1	0.883	8.85	-1.078	41.06
19	3	1	3	2	1	3	2	1	3	2	1.135	3.73	1.099	48.56
20	3	1	3	2	2	1	3	2	1	3	1.112	2.58	0.925	51.76
21	3	1	3	2	3	2	1	3	2	1	1.026	5.46	0.227	45.25
22	3	2	1	3	1	3	2	2	1	3	1.113	3.27	0.929	49.72
23	3	2	1	3	2	1	3	3	2	1	0.916	7.48	-0.765	42.52
24	3	2	1	3	3	2	1	1	3	2	1.066	5.39	0.558	45.37
25	3	3	2	1	1	3	2	3	2	1	0.999	5.36	-0.005	45.42
26	3	3	2	1	2	1	3	1	3	2	0.971	7.37	-0.259	42.65
27	3	3	2	1	3	2	1	2	1	3	1.068	2.84	0.571	50.94

Based on the maximization of  $T^*$  and minimization of  $C_t$ , the optimal combination of identified parameters is determined, a confirmation test is conducted, and the results are reported in the same Table 4. The influence rank of the parameter on both responses is almost the same, and in which, the mass flow rate of water entering the pipe ranks first position. However, the percentage contribution of each parameter to the output response has been calculated through the ANOVA technique.

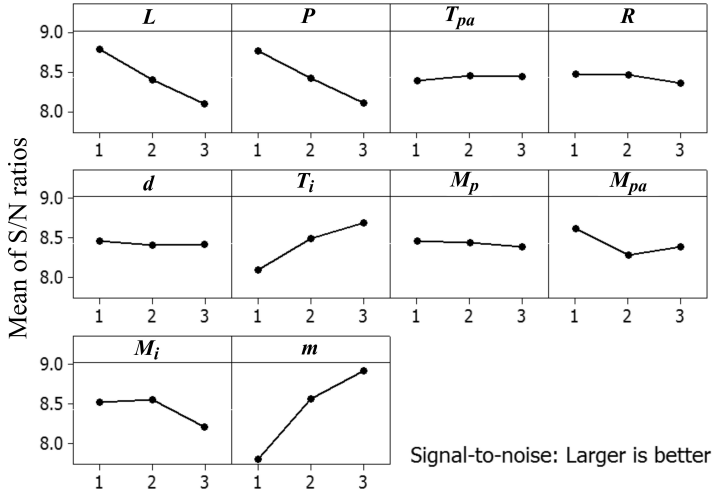


FIG. 5. Mean of  $S/N$  ratios for objective function  $T^*$ .

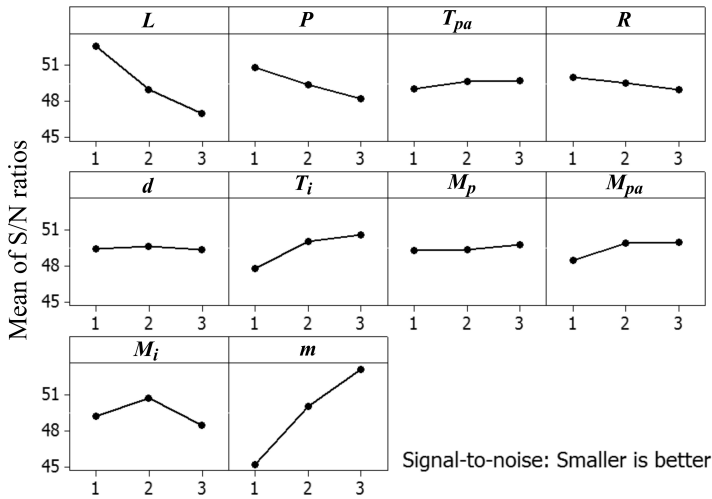


FIG. 6. Mean of  $S/N$  ratios for objective function  $C_t$ .

Table 4. Optimization result.

	Parameter	$L$	$P$	$T_{pa}$	$R$	$d$	$T_i$	$M_p$	$M_{pa}$	$M_i$	$m$	$T^*$	$C_t \cdot 10^{-4}$
Best levels	$T^*$	1	1	2	1	1	3	1	1	2	3	1.32	8.9
	$C_t$	1	1	3	1	2	3	3	3	2	3	1.27	8.3
Rank	$T^*$	2	3	9	7	10	4	8	6	5	1	–	–
	$C_t$	2	4	8	7	10	3	9	6	5	1	–	–

### 4.3. Analysis of variance (ANOVA)

ANOVA technique is used to investigate which design parameters significantly affect the quality characteristic [33]. Generally, the ANOVA method is employed to separate the total variability of the  $S/N$  ratio into contributions by each geometric parameter of the cooling panel and error. The sum of the squared deviations from the total mean  $S/N$  ratio is the total variability of the  $S/N$  ratio. In this study, the ANOVA analysis is conducted, and the results are given in Tables 5 and 6. From the ANOVA study, the mass flow rate of water entering the

**Table 5.** ANOVA result for  $T^*$ .

Source	Degree of freedom	Sum of square	Mean square	Variance ratio	Probability of significance	Percentage of influence
$L$	2	0.03335	0.016677	69.14	0	17.16
$P$	2	0.02981	0.014907	61.81	0	15.34
$T_{pa}$	2	6.05E-05	3.03E-05	0.13	0.884	0.03
$R$	2	0.00128	0.000644	2.67	0.148	0.66
$d$	2	7.03E-05	3.51E-05	0.15	0.867	0.04
$T_i$	2	0.02437	0.012186	50.53	0	12.54
$M_p$	2	0.00022	0.000114	0.47	0.645	0.12
$M_{pa}$	2	0.00791	0.003959	16.42	0.004	4.07
$M_i$	2	0.00943	0.004718	19.56	0.002	4.85
$m$	2	0.08783	0.043916	182.09	0	45.19
Error	6	0.00144	0.000241			
Total	26	0.19581				

**Table 6.** ANOVA result for  $C_t$ .

Source	Degree of freedom	Sum of square	Mean square	Variance ratio	Probability of significance	Percentage of influence
$L$	2	21.4262	10.7131	29.12	0.001	21.14
$P$	2	5.1392	2.5696	6.99	0.027	5.07
$T_{pa}$	2	3.3942	1.6971	4.61	0.061	3.35
$R$	2	0.2083	0.1042	0.28	0.763	0.20
$d$	2	0.5498	0.2749	0.75	0.513	0.54
$T_i$	2	10.1492	5.0746	13.79	0.006	10.01
$M_p$	2	0.2071	0.1036	0.28	0.764	0.20
$M_{pa}$	2	0.8607	0.4303	1.17	0.372	0.85
$M_i$	2	7.0725	3.5363	9.61	0.013	6.98
$m$	2	52.3358	26.1679	71.14	0	51.65
Error	6	2.2072	0.3679			
Total	26	103.5503				

pipe is identified as the most influencing parameter on both  $T^*$  and  $C_t$ , and its percentage of contribution is 45% and 50%, respectively. The length of the pipe influences about 17% on  $T^*$  and 21% on  $C_t$ . The pipe spacing influences 15% on the  $T^*$ , and the insulation layer thickness contributes about 10% on  $C_t$ . Rest of the factor's contribution is not significant in both the responses  $T^*$  and  $C_t$ . From this analysis, the designer or researcher may concentrate only on the most influencing parameters to improve the performance of the cooling panel system.

## 5. OPTIMIZATION BY THE GREY RELATIONAL METHOD

In the DOE optimization method, the best parameters for maximum  $T^*$  and minimum  $C_t$  are found out separately. However, the single parametric value that satisfies both maximizations of  $T^*$  and minimization of  $C_t$  can be obtained only through the grey relational method. Hence as the second part of this work, Taguchi's grey relational method is employed. The method of grey relational technique is shown in Fig. 7.

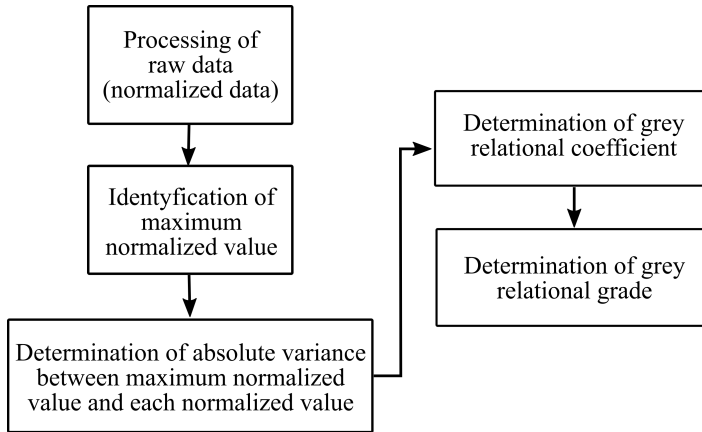


FIG. 7. Flow chart for the grey relational method.

Generally, normalization of raw data can be done through three different approaches based on the objective function [34]. In this study, the predicted  $T^*$  and  $C_t$  values for the 27 cases are normalized within the range of 0 to 1 using Eqs (5.1) and (5.2), and this step is referred to as data preprocessing. Now, the original sequence is transferred to the comparable sequence.

For the quality, the objective is maximization: larger the better

$$(5.1) \quad x_i^* = \frac{x_i^0(k) - \min x_i^0(k)}{\max x_i^0(k) - \min x_i^0(k)}, \quad k = 1, 2, \dots, n.$$

For the quality objective is minimization: smaller the better

$$(5.2) \quad x_i^* = \frac{\max x_i^0(k) - x_i^0(k)}{\max x_i^0(k) - \min x_i^0(k)}, \quad i = 1, 2, \dots, m,$$

where  $x_i^0$  is the value after the grey relational generation,  $\max x_i^0(k)$  is the largest value of  $x_i^0(k)$ ,  $\min x_i^0(k)$  is the smallest value of  $x_i^0(k)$  and  $x^0$  is the desired value. Also,  $m$  is the number of experiments and  $n$  is the total number of observations of data.

**Table 7.** Normalized data and grey relational coefficient.

Exp. No	$T^*$	$C_t$	Normalized data		GRC		Average GRC
			$T^*$	$C_t$	$T^*$	$C_t$	
1	1.09	0.005110	0.58	0.48	0.55	0.49	0.52
2	1.20	0.001464	0.89	0.95	0.83	0.91	0.87
3	1.24	0.001081	0.99	1.00	1.00	1.00	1.00
4	1.12	0.002029	0.66	0.88	0.59	0.80	0.70
5	1.17	0.001607	0.80	0.93	0.71	0.88	0.80
6	1.12	0.003844	0.67	0.64	0.60	0.58	0.59
7	1.08	0.002470	0.55	0.82	0.53	0.74	0.63
8	1.05	0.004460	0.47	0.56	0.49	0.53	0.51
9	1.12	0.002004	0.66	0.88	0.59	0.81	0.70
10	1.22	0.001736	0.94	0.92	0.90	0.86	0.88
11	1.03	0.005334	0.41	0.45	0.46	0.48	0.47
12	1.11	0.003535	0.63	0.68	0.58	0.61	0.59
13	0.98	0.005263	0.29	0.46	0.41	0.48	0.45
14	1.13	0.002473	0.70	0.82	0.63	0.74	0.68
15	1.15	0.002836	0.75	0.77	0.66	0.69	0.68
16	1.07	0.003870	0.52	0.64	0.51	0.58	0.55
17	1.19	0.002400	0.86	0.83	0.78	0.75	0.76
18	0.88	0.008847	0.01	0.00	0.34	0.33	0.33
19	1.13	0.003733	0.71	0.66	0.63	0.59	0.61
20	1.11	0.002582	0.65	0.81	0.59	0.72	0.65
21	1.03	0.005462	0.41	0.44	0.46	0.47	0.46
22	1.11	0.003267	0.65	0.72	0.59	0.64	0.61
23	0.92	0.007482	0.10	0.18	0.36	0.38	0.37
24	1.07	0.005390	0.52	0.45	0.51	0.47	0.49
25	1.00	0.005358	0.33	0.45	0.43	0.48	0.45
26	0.97	0.007373	0.25	0.19	0.40	0.38	0.39
27	1.07	0.002838	0.52	0.77	0.51	0.69	0.60

After preprocessing the raw data, the grey relation coefficient for the response characteristics should be calculated [40]. The grey relational coefficient is calculated from Eq. (5.3). The grey relational coefficient is calculated to express the relationship between the ideal and actual normalized experimental results

$$(5.3) \quad \xi_i(k) = \frac{\Delta_{\min} + \xi \cdot \Delta_{\max}}{\Delta_{0i}(k) + \xi \cdot \Delta_{\max}},$$

where  $\Delta_{0i}(k)$  is the deviation sequence of the reference sequence  $x_0^*(k)$ ,  $x_i^*$  is the comparability sequence, and  $\xi$  is the distinguishing or identification coefficient, which is generally employed as 0.5 in most of the studies. From the grey relational coefficients (GRC), the grey relational grade (GRG) is calculated using Eq. (5.4), and it is given in Table 7. The grey relational grades are used to show the relationship between the sequences

$$(5.4) \quad \gamma_i = \frac{1}{n} \sum_{k=1}^n \xi_i(k).$$

The mean response table for the overall grey relational grade is calculated and given in Table 8. The best values for the parameters have been identified from the response table and given in Table 8.

**Table 8.** Response table and best values.

Level	$L$	$P$	$T_{pa}$	$R$	$d$	$T_i$	$M_p$	$M_{pa}$	$M_i$	$m$
1	0.7019	0.6727	0.6114	0.626	0.5995	0.5405	0.5909	0.6037	0.5903	0.4616
2	0.5987	0.5961	0.6077	0.607	0.6111	0.6221	0.6064	0.598	0.6517	0.6208
3	0.516	0.5479	0.5975	0.5837	0.606	0.654	0.6195	0.615	0.5746	0.7343
Delta	0.1859	0.1247	0.014	0.0423	0.0117	0.1135	0.0286	0.0169	0.0771	0.2727
Rank	2	3	9	6	10	4	7	8	5	1
Best level	1	1	1	1	2	3	3	3	2	3

Finally, a confirmation test is conducted with the best set value from the multi-objective optimization, and the corresponding  $T^*$  and  $C_t$  values are found as 1.276 (radiant cooling panel average bottom temperature of 21.6°C) and  $1 \cdot 10^{-5}$ .

## 6. CONCLUSIONS

In this study, a radiant cooling panel was analyzed with a wave-shape pipe pattern embedded in the panel. The panel was fitted underneath the roof made of concrete, and in between, an insulation material layer was laid to arrest the

undesirable transfer of heat into the building. Numerical simulation technique: computational fluid dynamics method was employed to study the performance of the cooling panel through Fluent software. Three-dimensional model was created in the Gambit software, and meshed with tetrahedral T-grid type element.

Further, the numerical simulation made in Fluent software was also validated. The performance of the radiant cooling panel was studied through the average temperature on the bottom surface of the radiant cooling panel and temperature non-uniformity coefficient. The performance of the cooling panel was further enhanced through Taguchi's optimization technique. At first, the single objective optimization method was employed for the maximization of  $T^*$  and minimization of  $C_t$ . Later, multi-objective optimization was carried out through Taguchi's grey relational analysis with equal weight on both responses. Ten parameters were identified, varied through three levels of values, and the L27 orthogonal array was used. The best benefits of the defined parameters were analyzed through the  $S/N$  ratio and the grey relational coefficient for single and multi-objective, respectively. The determined best parameter value kept the average temperature of the panel bottom as  $21.6^\circ\text{C}$  for an indoor and outdoor temperature of  $27.5$  and  $67^\circ\text{C}$  respectively, and the temperature non-uniformity coefficient as  $1 \cdot 10^{-5}$ . Also, from the ANOVA analysis, the most influencing parameters on cooling panel performance were pipe length and mass flow rate of water.

## REFERENCES

1. SEVILGEN G., KILIC M., Numerical analysis of air flow, heat transfer moisture transport and thermal comfort in a room heated by two-panel radiators, *Energy and Buildings*, **43**(1): 137–146, 2011, doi: 10.1016/j.enbuild.2010.08.034.
2. NAGANO K., MOCHIDA T., Experiments on thermal environmental design of ceiling radiant cooling for supine human subjects, *Building and Environment*, **39**(3): 267–275, 2004, doi: 10.1016/j.buildenv.2003.08.011.
3. CATALINA T., VIRGONE J., KUZNIK F., Evaluation of thermal comfort using combined CFD and experimentation study in a test room equipped with a cooling ceiling, *Building and Environment*, **44**(8): 1740–1750, 2009, doi: 10.1016/j.buildenv.2008.11.015.
4. CHIANG W.H., WANG C.Y., HUANG J.S., Evaluation of cooling ceiling and mechanical ventilation systems on thermal comfort using CFD study in an office for subtropical region, *Building and Environment*, **48**: 113–127, 2012, doi: 10.1016/j.buildenv.2011.09.002.
5. JEONG J.W., MUMMA S.A., Practical cooling capacity estimation model for a suspended metal ceiling radiant cooling panel, *Building and Environment*, **42**(9): 3176–3185, 2007, doi: 10.1016/j.buildenv.2006.08.006.
6. KIM M.K., LEIBUNDGUT H., A case study on feasible performance of a system combining an airbox convector with a radiant panel for tropical climates, *Building and Environment*, **82**: 687–692, 2014, doi: 10.1016/j.buildenv.2014.10.012.

7. ZHANG L., LIU X.H., JIANG Y., Experimental evaluation of a suspended metal ceiling radiant panel with inclined fins, *Energy and Buildings*, **62**: 522–529, 2013, doi: 10.1016/j.enbuild.2013.03.044.
8. ZARRELLA A., DE CARLI M., PERETTI C., Radiant floor cooling coupled with dehumidification systems in residential buildings: A simulation-based analysis, *Energy Conversion and Management*, **85**: 254–263, 2014, doi: 10.1016/j.enconman.2014.05.097.
9. SU L., LI N., ZHANG X., Experimental study on cooling characteristics of concrete ceiling radiant cooling panel, *Procedia Engineering*, **121**: 2168–2175, 2015, doi: 10.1016/j.proeng.2015.09.089.
10. SU L., LI N., ZHANG X., SUN Y., QIAN J., Heat transfer and cooling characteristics of concrete ceiling radiant cooling panel, *Applied Thermal Engineering*, **84**: 170–179, 2015, doi: 10.1016/j.applthermaleng.2015.03.045.
11. ZHANG X., LI N., SU L., SUN Y., QIAN J., Experimental study on the characteristics of non-steady state radiation heat transfer in the room with concrete ceiling radiant cooling panels, *Building and Environment*, **96**: 157–69, 2016, doi: 10.1016/j.buildenv.2015.11.006.
12. OXIZIDIS S., PAPADOPOULOS A.M., Performance of radiant cooling surfaces with respect to energy consumption and thermal comfort, *Energy and Buildings*, **57**: 199–209, 2013, doi: 10.1016/j.enbuild.2012.10.047.
13. CHOLEWA T., ANASIEWICZ R., SIUTA-OLCHA A., SKWARCZYŃSKI M.A., On the heat transfer coefficients between heated/cooled radiant ceiling and room, *Applied Thermal Engineering*, **117**: 76–84, 2017, doi: 10.1016/j.applthermaleng.2017.02.019.
14. XIE D., WANG Y., WANG H., MO S., LIAO M., Numerical analysis of temperature non-uniformity and cooling capacity for capillary ceiling radiant cooling panel, *Renewable Energy*, **87**(3): 1154–1161, 2016, doi: 10.1016/j.renene.2015.08.029.
15. VANGTOOK P., CHIRARATTANANON S., Application of radiant cooling as a passive cooling option in hot humid climate, *Building and Environment*, **42**(2): 543–556, 2007, doi: 10.1016/j.buildenv.2005.09.014.
16. AN J.Y., KIM S., KIM H.J., SEO J., Emission behavior of formaldehyde and TVOC from engineered flooring in under heating and air circulation systems, *Building and Environment*, **45**(8): 1826–1833, 2010, doi: 10.1016/j.buildenv.2010.02.012.
17. MAEREFAT M., ZOLFAGHARI A., Omidvar A., On the conformity of floor heating systems with sleeping in the eastern-style beds; physiological responses and thermal comfort assessment, *Building and Environment*, **47**: 322–329, 2012, doi: 10.1016/j.buildenv.2011.07.008.
18. LEUNG C., GE H., Sleep thermal comfort and the energy-saving potential due to reduced indoor operative temperature during sleep, *Building and Environment*, **59**: 91–98, 2013, doi: 10.1016/j.buildenv.2012.08.010.
19. TIAN Z., LOVE J.A., Energy performance optimization of radiant slab cooling using building simulation and field measurements, *Energy and Buildings*, **41**(3): 320–330, 2009, doi: 10.1016/j.enbuild.2008.10.002.
20. ZEILER W., BOXEM G., Effects of thermal activated building systems in schools on thermal comfort in winter, *Building and Environment*, **44**(11): 2308–2317, 2009, doi: 10.1016/j.buildenv.2009.05.005.

21. MEMON R.A., CHIRARATTANANON S., VANGTOOK P., Thermal comfort assessment and application of radiant cooling: A case study, *Building and Environment*, **43**(7): 1185–1196, 2008, doi: 10.1016/j.buildenv.2006.04.025.
22. SONG D., KATO S., Radiational panel cooling system with continuous natural cross ventilation for hot and humid regions, *Energy and Buildings*, **36**(12): 1273–1280, 2004, doi: 10.1016/j.enbuild.2003.07.004.
23. LIM J.H., JO J.H., KIM Y.Y., YEO M.S., KIM K.W., Application of the control methods for radiant floor cooling system in residential buildings, *Building and Environment*, **41**(1): 60–73, 2006, doi: 10.1016/j.buildenv.2005.01.019.
24. YUAN Y L., ZHOU X., ZHANG X., Experimental study of heat performance on ceiling radiant cooling panel, *Procedia Engineering*, **121**: 2176–2183, 2015, doi: 10.1016/j.proeng.2015.09.090.
25. NIU J., KOOI J.V.D., Indoor climate in rooms with cooled ceiling systems, *Building and Environment*, **29**(3): 283–290, 1994, doi: 10.1016/0360-1323(94)90024-8.
26. MYHREN J.A., HOLMBERG S., Flow patterns and thermal comfort in a room with panel, floor and wall heating, *Energy and Buildings*, **40**(4): 524–536, 2008, doi: 10.1016/j.enbuild.2007.04.011.
27. HAO X., ZHANG G., CHEN Y., ZOU S., MOSCHANDREAS D.J., A combined system of chilled ceiling, displacement ventilation and desiccant dehumidification, *Building and Environment*, **42**(9): 3298–3308, 2007, doi: 10.1016/j.buildenv.2006.08.020.
28. KIM T., KATO S., MURAKAMI S., RHO J.W., Study on indoor thermal environment of office space controlled by cooling panel system using field measurement and the numerical simulation, *Building and Environment*, **40**(3): 301–310, 2005, doi: 10.1016/j.buildenv.2004.04.010.
29. DONGXIA Y., XIAOYAN L., DINGYONG H., ZUOREN N., HUI H., Optimization of weld bead geometry in laser welding with filler wire process using Taguchi's approach, *Optics & Laser Technology*, **44**(7): 2020–2025, 2012, doi: 10.1016/j.optlastec.2012.03.033.
30. SCHELLEN L., TIMMERS S., LOOMANS M., NELISSEN E., HENSEN J.L.M., VAN MARKEN LICHTENBELT W., Draught assessment during design: Experimental and numerical evaluation of a rule of thumb, *Building and Environment*, **57**: 290–301, 2012, doi: 10.1016/j.buildenv.2012.04.011.
31. TAGUCHI G., Introduction to quality engineering, *Asian Productivity Organization APO*, Tokyo, Japan, 1990.
32. MANIVEL D., GANDHINATHAN R., Optimization of surface roughness and tool wear in hard turning of austempered ductile iron (grade 3) using Taguchi method, *Measurement*, **93**: 108–116, 2016, doi: 10.1016/j.measurement.2016.06.055.
33. KOKSAL S., FICICI F., KAYIKCI., SAVAS O., Experimental optimization of dry sliding wear behavior of in situ AlB<sub>2</sub>/Al composite based on Taguchi's method, *Materials and Design*, **42**: 124–130, 2012, doi: 10.1016/j.matdes.2012.05.048.
34. ÇAYDAŞ U., HAŞÇALIK A., Use of the grey relational analysis to determine optimum laser cutting parameters with multi-performance characteristics, *Optics and Laser Technology*, **40**(7): 987–994, 2008, doi: 10.1016/j.optlastec.2008.01.004.

35. ARCURI N., BRUNO R., BEVILACQUA P., Influence of the optical and geometrical properties of indoor environments for the thermal performances of chilled ceilings, *Energy and Buildings*, **88**: 229–237, 2015, doi: 10.1016/j.enbuild.2014.12.009.
36. PRAKASH D., Thermal analysis of building roof assisted with water heater and insulation material, *Sādhanā*, **43**: 30, 2018, doi: 10.1007/s12046-017-0781-y.
37. SHEN L., TU Z., HU Q., TAO C., CHEN H., The optimization design and parametric study of thermoelectric radiant cooling and heating panel, *Applied Thermal Engineering*, **112**: 688–697, 2017, doi: 10.1016/j.applthermaleng.2016.10.094.
38. ROMANÍ J., BELUSKO M., ALEMU A., CABEZA L.F., DE GRACIA A., BRUNO F., Optimization of deterministic controls for a cooling radiant wall coupled to a PV array, *Applied Energy*, **229**: 1103–1110, 2018, doi: 10.1016/j.apenergy.2018.08.035.
39. JOE J., KARAVA P., A model predictive control strategy to optimize the performance of radiant floor heating and cooling systems in office buildings, *Applied Energy*, **245**: 65–77, 2019, doi: 10.1016/j.apenergy.2019.03.209.
40. NAYAK S.K., PATRO J.K., DEWANGAN S., GANGOPADHYAY S., Multi-objective optimization of machining parameters during dry turning of AISI 304 austenitic stainless steel using grey relational analysis, *Procedia Materials Science*, **6**: 701–708, 2014, doi: 10.1016/j.mspro.2014.07.086.

*Received February 22, 2019; accepted version September 9, 2019.*

---

*Published on Creative Common licence CC BY-SA 4.0*

